Eur. Phys. J. D (2023) 77:103
https://doi.org/10.1140/epjd/s10053-023-00680-y

THE EUROPEAN PHYSICAL JOURNAL D

Regular Article – Atomic and Molecular Collisions

The Xe autoionizing states in kinetic energy region (3–14) eV studied at high and low incident electron energies

Jozo J. Jureta[1,a], Bratislav P. Marinković[1,b], and Lorenzo Avaldi[2,c]

[1] Laboratory for Atomic Collision Processes, Institute of Physics Belgrade, University of Belgrade, Pregrevica 118, 11080 Belgrade, Serbia
[2] CNR-Istituto di Struttura della Materia, Area della Ricerca di Roma 1, CP10, 00015 Monterotondo Scalo, Italy

Received 31 March 2023 / Accepted 23 May 2023 / Published online 14 June 2023

Abstract. The spectra of the autoionizing states of xenon have been measured at high (505, 2019) eV and low (24–60) eV incident electron energies and ejection angle at 90° using high-resolution electron spectroscopy. A wealth of peaks and dips which correspond to the singly, doubly excited states, and slow Auger electrons are detected in the kinetic energy region (3–14) eV in the spectrum measured at 505 eV. Each feature is analyzed systematically, the energy and assignment are defined in comparison with corresponding structures reported in literature. The main attention has been focused to obtain energies of the triplet states less known from literature. Energies of the triplet $5s5p^6$ (6s, 7s, 6p, 5d) states are obtained combining the data from high and low incident energies. In addition, angular dependence of the features at low incident energies 24, 26 and 30 eV are presented.

1 Introduction

Electron impact experiment is a powerful tool to investigate the electronic structure of atoms and molecules as well as the single and multiple ionization processes (Märk and Dunn [1]). Electron–electron cocincidence technique then add extra selectivity and allowes to study finer details of the electron-atom interaction, like for example non isotropic post collision interaction (PCI) which determine shapes and angular dependence of Auger lines (Avaldi et al. [2]). However, ejected electron spectroscopy studies with electrons as projectiles are much scarcer than the corresponding studies with photons. The aim of this paper is to provide an extensive identification of autoionizing lines of the xenon atom observed by electron impact using ejected electron spectroscopy in the region of kinetic energies lower than 14 eV. Primary electron beams with energies varying from 2019 to 24.2 eV have been used, while the ejected electrons are analyzed in energy and angle.

The Xe autoionizing states induced by electrons at high incident energies have been recently studied via Auger transitions (Jureta et al. [3] and references therein), while studies at low incident electron energies are rare: Brion and Olsen [4], Tweed et al. [5], and Delage et al. [6]. Although threshold electron spectroscopy with low resolution has been used in [4], their calculated energies for most of the excited $(5s6p^5)ns$, nd states are in a good agreement with the present experimental results. In [5], both ejected and scattered electrons in a limited kinetic energy region (8–12) eV at 100 eV incident energy and ejection angles 0° and 80° have been studied at low resolution. In [6], the excitation functions of the 6s, 6s', 6p and 5d states in energy region (18–24) eV have been studied by using electrostatic spectrometer in the energy loss mode.

The first Xe autoionizing spectra in photo-absorption experiments have been reported by Samson [7] and Codling and Madden [8]. After these experiments attention has been paid to the investigations of the photoelectron spectra with the aim to explain correlation satellites associated with the 5s line that appeared as series of structures. These structures in the spectra are a consequence of the excitation of different final ion states resulting from electron correlation effects: Gelius [9], Svensson et al. [10], Carlsson-Gothe et al. [11] and Hansen and Persson [12].

Photoelectron spectroscopy with synchrotron radiation has been widely used to study the satellite lines and dynamics of the Auger decay of the 4d shell: Fahlman et al. [13], Krause et al. [14], Brion et al. [15], Southworth et al. [16], Wills et al. [17], Kikas et al. [18], Kivimäki et al. [19], Jauhiainen et al. [20], Alitalo et al. [21], Huttula et al. [22], Ueda et al. [23], Lablanquie

[a] e-mail: jureta@ipb.ac.rs
[b] e-mail: bratislav.marinkovic@ipb.ac.rs (corresponding author)
[c] e-mail: lorenzo.avaldi@ism.cnr.it

et al. [24], Penent et al. [25], Jonauskas et al. [26] and Becker et al. [27].

The study of correlation satellites in the kinetic energy region (7–14) eV excited by electrons were performed experimentally by Aksela et al. [28] who used a cylindrical mirror spectrometer with a non-monochromatic electron beam. They also employed theoretical estimates based on Dirac–Fock multiconfiguration computation. King et al. [29] investigated the structures near the Xe $N_{4,5}$ edges by using high resolution electron beam at incident energy of 1.5 keV. Theoretical calculations were done by Dyall and Larkins [30] and Petrov et al. [31]. Braidwood et al. [32] and Brunger[1] et al. [33] studied the satellite structure of valence shells and 4d core states by electron-momentum spectroscopy, respectively.

In the present work we have studied the Xe autoionizing spectra in the kinetic energy region (3–14) eV obtained at high (505, 2019) eV at 90° and low incident electron energies (24–60) eV at 40°, 90° and 130°. The incident electron energy of 2019 eV have been chosen to allow us seeing all contributions from M subshell excitations, while at the energy of 505 eV all of these contributions are excluded and only those coming from N and O subshells are present in ejected electron spectra. The angular dependence of the Auger lines due to PCI effect has been theoretically predicted (c.f. [2]). All obtained features are analyzed, most of them assigned in comparison with the corresponding structures from Ref-s presented in Table 1.

2 Experimental

Details about the experimental setup may be found in Jureta et al. [34] and will not be repeated here. In the experiment a non-monochromatic electron beam tunable in the energy region (24–2019) eV (± 0.4 eV) collides with an atomic beam effusing from the platinum-iridium non-biased needle (ID = 0.5 mm) in the perpendicular direction to the scattering plane. Two cylinders made of thin μ-metal foils define the interaction region with diameter of 50 mm. The cylinders are separated by 10 mm gap in the collision plane in order to avoid collection of scattered electrons from metal surfaces.

The ejected electrons after passing through a high-resolution hemispherical analyzer (OMICRON EA125 SHR U7) with a mean radius of 125 mm are detected by seven channeltrons. The analyzer operates at pass energy mode of 1 eV with defined retarding ratio and magnification determined by a two stage 11-element lens system. The spectra shown in the figures are obtained in the Constant Analyzer Energy (CAE) mode. In this mode, the analyzer pass energy is fixed in order to keep the resolution constant, while the kinetic energy is scanned by varying the retarding ratio of the lens stack. The background and working pressures in the vacuum chamber were 6×10^{-8} and 2×10^{-6} mbar, respectively. The accumulation time was roughly 1 h for most of the spectra with an energy step of 0.020 eV.

The best resolution, defined as full width at half maximum (FWHM), measured in the spectrum is 125 ± 20 meV at high energy and 80 to 100 meV at low energy including natural width of the state. The transmission was not uniform, and all spectra are presented with subtracted background.

The calibration of the kinetic energy was performed using a Xe-Ar mixture and the energy position of the $3d(^1D)$ state of argon at 11.72 eV observed with an uncertainty of (± 0.02) eV [35]. The incident energy scale was calibrated using the elastic scattered electrons with a typical FWHM of (0.80 ± 0.40) eV.

3 Results and discussion

3.1 Autoionizing spectra of xenon at high incident electron energy

Figure 1a shows the autoionizing spectrum of xenon obtained at 505 eV in kinetic energy region from 3 to 14 eV. In the inset the spectrum in kinetic energy region 3–8.6 eV obtained at 2019 eV incident energy is also shown. Both spectra are measured at 90°. The incident energy of 505 eV is below the binding energy of the 3d shell (680 eV). Thus, all features result from the ionization of the 4d, 4p and 4s inner shells, while the spectrum at the incident energy of 2019 eV can include the contribution from the 3d shell ionization. In such manner it is possible to follow the appearance of structures, find out their origins and propose their assignments. It is to be noted that the spectrum that covers low kinetic energy range at high incident electron energies has not been published before.

The first two features (1, 2) at 3.14 and 3.38 eV, respectively, shown in the spectra have low intensities. This makes difficult to identify their origin. In comparison with Lablanquie et al. [24, Fig. 6] one can see that the energy of the feature (1) is close to the energy of the small structure at 3.2 eV originated from a decay of the $4d_{3/2}$ subshell. They concluded that this structure appears in the Xe^{3+} continuum formed by the double Auger process. Another assignment for this feature is proposed by the calculation in [31] as the transition N_4-$5p^2(^1S)5d^2(^3P)(^3P_0)$. On the other side, as shown in Fig. 1b, the feature (1) noticeable at 505 eV vanishes below 300 eV indicating its origin from ionization of the 4s shell. Thus, despite the very good agreement in energies that assignment is not accepted. Feature (2) at 3.38 eV is visible at 2019 eV but not at 505 eV (Fig. 1a). This indicates its origin is probably from ionization of the 3d shell around 700 eV. The feature is left without assignment due to the absence of data from

[1] This study commemorates the work of Prof. M.J. Brunger, a colleague and great scientist who recently passed away.

Table 1 Kinetic energies (KE) of the peaks and dips from the Xe ejected electron spectra spectra taken from Fig. 1a

This work peaks, Dips N^0 KE(eV)	Energy difference between peaks ΔE (eV)	[Ref.], Line: Assignment	Kinetic En. (KE) or Binding En. (BE) (eV)*
1 3.14	(1–2): 0.24	[24], $(4d_{3/2})^{-1} \rightarrow Xe^{2+} \rightarrow Xe^{3+}$	3.2
		[31], N_4-$5p^2(^1S)5d^2(^3P)(^3P_0)$	3.17
2 3.38		[24], $(4d_{3/2})^{-1} \rightarrow Xe^{2+} \rightarrow Xe^{3+}$	3.4
3 3.52	(3–4): 0.22	[24], $(4d_{3/2})^{-1} \rightarrow Xe^{2+}$(A)	3.6
		[25], $(4d_{3/2})^{-1} \rightarrow Xe^{2+}$(A)	3.5
4 3.74	(4–11): 2.02	[22], (5d): Xe $4d_{5/2}6p \rightarrow 5p^4(^1D_2)$	5.67
11 5.76		[24], $(4d_{3/2})^{-1} \rightarrow Xe^{2+} \rightarrow Xe^{3+}$	3.8
		[31], N_4-$5p^2(^1D)5d^2(^1D)(^1S_0)$	3.67
5 3.94		[24], $(4d_{5/2})^{-1} \rightarrow Xe^{2+} \rightarrow Xe^{3+}$	3.9
6 4.06		[24], $(4d_{3/2})^{-1} \rightarrow Xe^{2+} \rightarrow Xe^{3+}$	4.1
7 4.22			
8 4.46		[31], N_5-$5p^2(^1D)5d^2(^3F)(^3P_0)$	4.49
9 4.70		[24], $(4d_{5/2})^{-1} \rightarrow Xe^{2+}$	4.70
10 5.30		[24], $(4d_{5/2,\ 3/2})^{-1} \rightarrow Xe^{2+}$	5.4
12 6.20	(12–16): 1.32	[This work], (12, 16): $5s5p^66s(^3S)$	19.645*
16 7.52	(12–13): 0.41	[4], $5s5p^66s(^3S)$	19.80*
		[5], $5s5p^66s$ (J = 1)	19.40*
		[22], 9a: Xe $4d_{5/2}6p \rightarrow 5p^4(^3P_2)$	7.53
		[24], $(4d_{5/2})^{-1} \rightarrow Xe^{2+}$	6.16
13 6.62	(13–19): 1.30	[This work], (13, 19): $5s5p^66s(^1S)$	20.055*
19 7.92	(16–19): 0.40	[4, 6, 38], $5s5p^66s$	(20.08, 20.02, 20.08)*
		[5], $5s5p^66s$ (J = 0)	19.88*
		[22], (7b, 2a): $4d_{5/2}6p \rightarrow 5p^4(^3P_{0,1},\ ^3P_2)$	(6.62, 7.93)
		[24], $(4d_{3/2})^{-1} \rightarrow Xe^{2+}$	6.7
14 6.88		[23], $5s^05p^6(^1S)6p \rightarrow 5s^15p^5\ ^3P_2$	6.86
15 7.42	(15–17): 0.22	[28], 5: . . . /.	7.45
17 7.64		[22, 23], (7a, b): Xe $4d_{5/2}6p \rightarrow 5p^4(^3P_2)$	7.63, 7.64
		[28], 6: . . . /.	7.67
18 7.78	(18–24): 1.32	[This work], (18, 24): $5s5p^65d(^3D)$	21.225*
24 9.10	(18–20): 0.22	[5], 4: $5s5p^65d$	21.22*
		[26], label 1: $4d^{-1}5p^{-1} \rightarrow 5s^{-1}5p^{-2}$	7.79
		[26], label 4: $4d^{-2} \rightarrow 4d^{-1}5s^{-1}5p^{-1}$	9.21
		[28], 10: . . . /.	9.11
20 8.00	(20–25): 1.32	[This work], (20, 25): $5s5p^65d(^1D)$	21.445*
25 9.32	(24–25): 0.22	[4, 6, 38], $5s5p^65d$	(21.30, 21.38 21.44)*
		[7, 8], (. . . , 9): . . . /.	(21.40, 21.408)*
		[28], 7: . . . /.	8.03
21 8.25	(21–29): 1.97	[16], (7, 6): $N_{5,4}$—$5s^05p^6(^1S_0)$	(8.24, 10.22)
29 10.22		[19], (1, 2): $N_{5,4}$—$O_1O_1(^1S_0)$	(8.26, 10.25)
		[20, 28], (1, 2; 8, 13):	(8.30, 10.27)
		($N_{5,4}$—$O_1O_1(^1S_0)$, . . . /..)	(8.32, 10.31)
		[36], (30, 29): $N_{5,4}$—$5s^25p^3(^2P)7$ s:$^1P_1$	(8.300, 10.279)
		[37], (30, 29)	

Table 1 (continued)

This work peaks, Dips N^0 KE(eV)	Energy difference between peaks ΔE (eV)	[Ref.], Line: Assignment	Kinetic En. (KE) or Binding En. (BE) (eV)*
22 8.41 26 9.70	(22- 26): 1.29	[This work], (22, 26): $5s5p^6 7s$ [4–6], $5s5p^6 7s$ [20, 39], 2: N_5-$5s^2 5p^3(^2D)6d\ ^3S_1$ [28], 9: . . . /.	21.84* (21.80, 21.72, 21.82)* (9.72, 9.77) 8.46
(a) 8.54 (a') 8.66 (a") 8.76 (a"') 8.86	(a–a"): 0.22	[This work], (a): [This work], (a"): $5s5p^6 6p(^1P)$ [4, 5], $5s5p^6 6p$ [6], (. . . /.., $5s5p^6 6p$) [7, 8], (1, 2, 3, 4): $5s5p^6 6p$	20.67* 20.89* (20.95, 20.95)* (20.67, 20.95)* (20.66, 20.80, 20.95, 21.03)*
		[26], label 3: $4s^{-1}4d^{-1} \rightarrow 4p^{-1}4d^{-1}5s^{-1}$	8.88
23 9.01		[This work], . . . /. [6], j: . . . /. [8], 5: . . . /.	21.14* 21.10* 21.147*
27 9.83 42 11.87	(27–42): 2.04	[28], (12, 17): . . . /.	(9.80, 11.89)
28 9.96 37 11.26	(28–37): 1.30	[This work], . . . /. [8], 60: . . . /. [11, 15], 5s5p ($^2S_{1/2}$)	23.395* 23.389* 23.397*
30 10.38		[This work], $5s5p^6 8s$ [4], $5s5p^6 8s$ [8], 22: $5p^4 6s7p$	22.51* 22.52* 22.511*
31 10.48 41 11.78	(31–41): 1.30	[This work], . . . /. [6, 8], t: . . . /..; 74: . . . /.	23.915* (23.91, 23.895)*
(b) 10.05		[This work], $5s5p^6 7p$ [5, 7], $5s5p^6 7p$ [8], (15, 16): . . . /.., $5s5p^6 7p$ [20, 39], 3: N_5—$5s^2 5p^3(^2D)6d\ ^3D_1$	22.18* (22.20, 22.223)* (22.188, 22.226)* (10.07, 10.05)
(c) 10.54		[This work], $5s5p^6 8p$ [5, 7], $5s5p^6 8p$ [8], (27, 28): . . . /.., $5s5p^6 8p$ [20], 5: . . . /.	22.67* (22.68, 22.701)* (22.671, 22.704)* 10.60
32 10.59		[This work], $5s5p^6 7d$ [4, 6], $5s5p^6 7d$ [20], 5: N_5—$5s^2 5p^3(^2D)6d\ ^3D_1$	22.72* (22.70, 22.73)* 10.60
33 10.70		[This work], $5s5p^6 9s$ [4],:$5s5p^6 9s$ [8], 33: . . . /.	22.83* 22.85* 22.813*
(d) 10.75		[This work], $5s5p^6 9p$ [5, 7],:$5s5p^6 9p$ [8], (34, 37): . . . /.., $5s5p^6 9p$ [26], label 6: $4d^{-2}5p^{-2} \rightarrow 4d^{-1}5p^{-4}$ [28], 14: . . . /.	22.88* (22.96, 22.93)* (22.877, 22.937)* 10.75 10.76
34 10.83 43 12.15	(34–43): 1.32	[This work], (34): $5s5p^6 8d$ [4, 6], (8, q): $5s5p^6 8d$,../. [8], 80: . . . /. [20, 39], 45: N_4-$5s^1 5p^5\ ^3P_2$	22.96* (22.95,22.99)* 24.289* (24.29, 24.26)*

Table 1 (continued)

This work peaks, Dips N^0 KE(eV)	Energy difference between peaks ΔE (eV)	[Ref.], Line: Assignment	Kinetic En. (KE) or Binding En. (BE) (eV)*
35 10.93		[This work], $5s5p^6 9d$	23.06*
		[4], $5s5p^6 9d$	23.07*
		[7], $5s5p^6 10p$	23.071*
		[8], 39: . . . /.	(23.056)*
		[20, 39], 6: N_5-$5s^2 5p^3(^2P)6p\ ^1S_0$	(10.96, 10.84)
36 11.08		[This work], $5s5p^6$ 11d	23.21*
		[4], $5s5p^6$ (11d, 12d)	(23.21, 23.24)*
		[6], . . . /.	23.26*
		[8], 48: . . . /.	23.206*
		[28], 15: . . . /.	11.01
(e) 11.43		[6, 8], s, 66:. . . /.	(23.59, 23.555)*
38 11.52		[15], *: . . . /.	23.7*
39 11.61		[20], 8: N_5-$5s^2 5p^3(^2P)6p\ ^3D_3$	(11.55, 11.57)
40 11.72		[20, 39], 9: N_4-$5s^2 5p^3(^2D)6d\ ^3S_1$	(11.69, 11.75)
(f) 12.08		[8], 79: . . . /.	24.201*
44 12.26		[26], label 7: $4d^{-2}5s^{-1}5p^{-1} \rightarrow 4d^{-1}5s^{-1}5p^{-3}$	12.26
45 12.45		[8], 88: . . . /.	24.581*
46 12.60		[8], (93): . . . /.	(24.73)*
47 12.68		[8], 95: . . . /.	24.810*
		[28], 19: . . . /.	12.68
48 12.76		[8], 96: . . . /.	24.869*
		[(19, 31), 20, 39],: (3, 12),	(12.72, 12.58),
		N_5—$5s^2 5p^3(^2P)5d\ ^1P_1$	12.77, 12.739
		[24, 28], N_5-$O_1O_{2,3}$	12.78, 12.85
		[36]: 28:. . . /.	12.54
		[37]: 28:. . . /.	12.741
49 12.84		[8], 99: . . . /.	24.991*
		[20, 28], 3, 20: (N_5—$5p^3$ 5d, . . . /..)	12.85
50 12.96		[8], 104: . . . /.	(25.078)*
		[23], Xe $4d_{5/2}6p \rightarrow 5s^0 5p^6(^1S)6p$	12.99
51 13.06		[This work]	25.19*
		[8], 108: . . . /.	25.195*
52 13.12		[This work]	25.25*
		[8], 109: . . . /.	25.240*
53 13.18		[This work]	25.31*
		[8], (111): . . . /.	25.307*
		[20, 24, 28], (13, 13, 21): $4d_{3/2,}$, . . . /.	13.15, 13.16, 13.16
54 13.32		[This work]	25.45*
		[8], (120): . . . /.	25.457*
55 13.5		[This work]	25.63*
		[8], 124: . . . /.	25.663*
56 13.64		[This work]	25.77*
		[8], 126: . . . /.	25.761*

Ref-s: Brion and Olsen [4], Tweed et al. [5], Delage et al. [6], Samson [7], Codling and Madden [8], Carlsson-Gothe et al. [11], Brion et al. [15], Southworth et al. [16], Kivimäki et al. [19], Jauhiainen et al. [20], Alitalo et al. [21], Huttula et al. [22], Ueda et al. [23], Lablanquie et al. [24], Penent et al. [25], Jonauskas et al. [26], H. Aksela et al. [28], Petrov et al. [31], Werme et al. [36], Carroll et al. [37], Bergmark et al. [38], Persson et al. [39]
(*) Binding energy

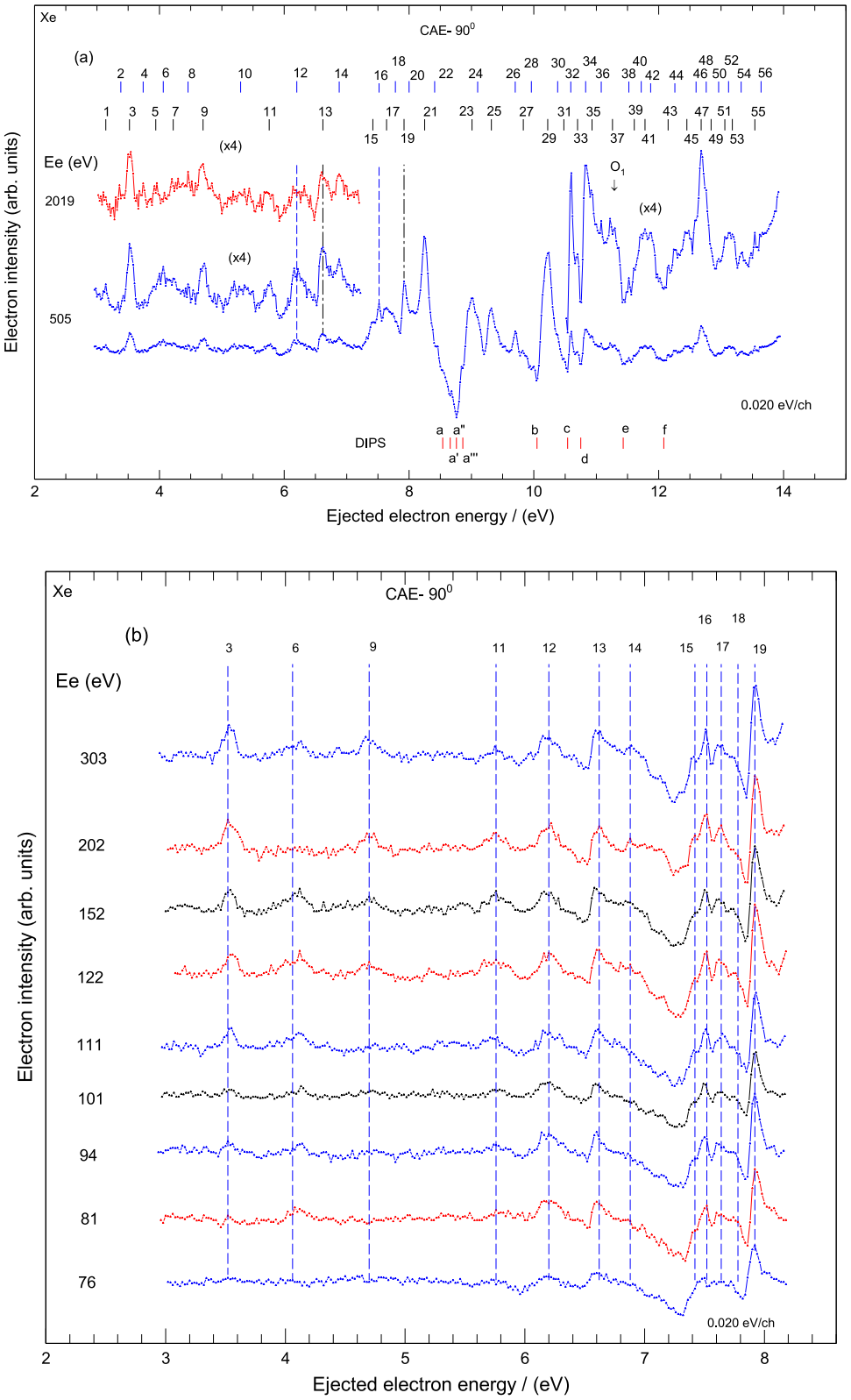

Fig. 1 **a** The Xe autoionizing spectrum in the kinetic energy region from 3 to 14 eV obtained in the CAE mode at 505 eV and ejection angle of 90°. Two parts of the spectrum are presented in enlarged scales to enhance features at low intensities. Short vertical lines at the top and bottom of the Figure show energy positions of the peaks and the dips, respectively. Long dashed lines show positions of the doublets arising from the $5s5p^6 6s$ state that decays to the two terms of the $^2P_{3/2,1/2}$ ion core. The energies of the peaks and dips with their proposed assignments are listed in Table 1. **b** Series of Xe electron ejected spectra obtained in the CAE mode at 90° in the kinetic energy region (3–8.2) eV and electron incident energies from 303 to 76 eV. The features are labeled as in Table 1

Jonauskas et al. [26] who have been studied experimentally and theoretically cascade satellites following ionization of the 3d shell. In comparison with [24, Fig. 6] one can notice that the energy of feature (2) is close to the energy of the small structure at about 3.4 eV recognized as a second step Auger electron coming from decay of the Xe^{2+} state formed by emission of a 2 eV Auger electron by decay of the $4d_{3/2}$ hole.

Feature (3) at 3.52 eV appearing as a single peak vanishes at incident energy below 76 eV (Fig. 1b) indicating its origin from ionization of the $4d_{3/2}$ subshell (69.54 eV). Ejected electron of 3.52 eV can be produced by the decay of the $4d_{3/2}$ subshell via the Xe^{2+} intermediate (A) state at 66 eV (labelled A in [25]) to the final $Xe^{3+}(^2D_{3/2})$ state (Penent et al. [25]). The process gives a total energy of 69.52 eV (3.52 + 66), in excellent agreement with energy of the $4d_{3/2}$ (69.54 eV) and this assignment is accepted. In [25, Fig. 3] the formation of the five final Xe^{3+} states through double Auger decay of the $4d_{3/2}$ subshell is presented. In the absence of numerical data, we suppose that the energy position of the peak $1A_2{}^{3/2}$ of [25, Fig. 3] between 3 and 4 eV kinetic energy is in good agreement with the position of the feature (3). Lablanquie et al. [24] presented in Fig. 6 an intense structure at 3.6 eV in Auger spectrum obtained in a coincidence experiment where an Auger electron and a threshold photoelectron from the $4d_{3/2}$ subshell ionization are detected. This suggests the formation of Xe^{2+} states embedded in the Xe^{3+} continuum. It is clear that our feature (3) corresponds to the structures observed in [24, 25], i.e., to a slow Auger electron created by a cascade process from ionization of the $4d_{3/2}$ subshell. Becker et al. [27, Fig. 1] observed a structure at around 3.6 eV in the photoelectron spectrum of Xe at 110 eV, but did not provide any assignment. This structure may also correspond to the feature (3). In all photoelectron spectra the energy of the structure around 3.6 eV was not precisely defined, but in the present experiment the energy is well defined at (3.52 ± 0.020) eV and it can serve as a calibration energy due to its observation even at 2019 eV. This is the first evidence of the cascade Auger process in xenon in experiment with electrons.

The features (4, 11) at 3.74 and 5.76 eV, respectively, observed at 2019 eV form a pair with energy separation of 2.02 eV, close to the energy splitting between 4d subshells (1.99 eV). For their assignment several possibilities are listed in Table 1. The peak (4) is observed only at the highest measured energy and it vanishes at 505 eV, while the peak (11) is present almost at all energies. It becomes weaker with decreasing energy and almost disappears at the lowest energy of 76 eV, as shown in Fig. 1b. A comparison with ref. [24, Fig. 6] shows that energy of the feature (4) is close to the energy of the structure at 3.8 eV created by decay of the $4d_{3/2}$ subshell embedded in the Xe^{3+} continuum. In the calculation of ref. [31] an energy of 3.74 eV is assigned to the N_4-$5p^2(^1D)5d^2(^1D)(^1S_0)$ line in the NOO Auger spectrum. Finally, the several proposals for feature (4) show that its assignment is still uncertain and waits for new measurements. On the other hand the energy of the feature (11) (5.76 eV) shows a good agreement with energy 5.67 eV of the peak 5d in Fig. 5c of Huttula et al. [22], which is assigned to the transition of the Xe $4d_{5/2}$ 6p to the $5p^4(^1D_2)$ state. In the case of [22], the energies of peaks in Fig. 5a, b, c are not tabulated, so we estimated them from the figures and therefore may be affected by some uncertainty.

The features (5, 6, 7, 8) at 3.94, 4.06, 4.22 and 4.46 eV, respectively appear as resolved features with low intensities at 2019 eV, but as a broad structure with maximum at 4.06 eV at 505 eV. The feature (5) (3.94 eV) is clearly visible at 2019 eV. This indicates its origin probably from ionization of the 3d shell. The energy however is close to the energy of the unresolved structure at about 3.9 eV in Fig. 6 of ref [24] created by decay of the $4d_{5/2}$ subshell embedded in the Xe^{3+} continuum. Feature (6) (4.06 eV) vanishes at around 76 eV of incident energy (Fig. 1b) indicating its origin from ionization of the 4d subshell, probably produced by decay of the $4d_{3/2}$ subshell observed in [24, Fig. 6] at 4.1 eV. It should be noted that the Auger lines in the $4d_{5/2}$ decay between 3.5 and 4 eV are not resolved in [24]. Feature (7) (4.22 eV) vanishes between 200 and 300 eV incident energy indicating its origin from ionization of the 4s shell, but it is left without assignment due to the absence of previous data. Feature (8) (4.46 eV) has an energy close to the energy 4.49 eV calculated in [31]. Its proposed assignment is not accepted because the feature vanishes between 200 and 300 eV.

Feature (9) (4.70 eV) is present in Fig. 1a as a single peak which vanishes at 76 eV indicating its origin from the ionization of one of the 4d subshells. Energy of this feature is equal to the energy of the Auger line at 4.7 eV in [24], assigned to the slow Auger electron produced from the decay of the $4d_{5/2}$ subshell via a cascade of the intermediate Xe^{2+} state at energy 62.85 eV (67.55–4.70), although this state is not listed in the energy level diagrams in Fig. 7 of [24] nor in Fig. 4 of [25].

Feature (10) (5.30 eV) is present at both energies as a broad structure which vanishes at incident energies between 300 and 200 eV, indicating its origin from ionization of the 4s state. However, the energy of this feature is close to the energy of the Auger lines at 5.4 eV presented in both spectra in [24, Fig. 6]. Finally, a comparison of the kinetic region from 3 to 5.5 eV from the present work with the corresponding regions in Huttula et al. [22, Fig. 1] and Lablanquie et al. [24, Fig. 6] shows considerable similarities.

The features (14, 15, 17) at 6.88, 7.42 and 7.64 eV, respectively, are not resolved from neighboring structure at 505 eV. Feature (14) vanishes below 80 eV (Fig. 1b) and can be attributed to the second step of Auger cascade transition from the excitation of the Xe $4d_{5/2}6p \rightarrow Xe^+ 5s^0 5p^6(^1S)6p \rightarrow Xe^{2+} 5s^1 5p^5\ ^3P_2$ state with energy of 6.86 eV [23]. Feature (15) vanishes at around 60 and its kinetic energy is in a very good agreement with the unassigned line (5) at 7.45 eV in Aksela et al. [28]. Feature (17) vanishes at 40 eV

indicating its origin from excitation of the state above Xe^{2+} (33.10 eV), again its kinetic energy is in very good agreement with the unassigned line (6) (7.67 eV) [28]. Also, its energy is in excellent agreement with energy of the peak (7a) 7.63 eV [22] and 7.64 eV [23] assigned as the second step Auger transition from the Xe $4d_{5/2}6p$ to the $5p^4(^3P_2)$ state. Since this feature is present in spectra even at energies below the excitation of the $4d_{5/2}6p$ state (65.11 eV) this assignment has not be accepted.

The pair of features (21, 29) (8.25, 10.22) eV with energy separation 1.97 eV are present in spectrum at 505 eV with high intensities and shapes affected by neighboring features. Energies of these features show an excellent agreement with energies of corresponding lines in [16, 19] which assignment is accepted. The lines (7, 6) in [16] and (1, 2) in [19] are the first pair of Auger lines as in [36, 37], but with different assignments in the last two references. The energies of corresponding lines (8, 13) in [28] are in good agreement with energies of our features (21, 29), but no assignments were given. In [20] energies of the lines (1, 2) are taken from [28] and assigned as Auger lines $N_{5,4}$–$O_1O_1(^1S_0)$.

Feature (23) at 9.01 eV is shown in the spectra as a broad asymmetric peak not resolved from feature (24) at 9.10 eV. It is present at all incident energies until 26 eV (see Fig. 2) where it becomes a narrow peak of low intensity. If the corresponding state decays to the term $^2P_{3/2}$ of ion core (12.13 eV), then the energy 21.14 eV of the (23) is in excellent agreement with corresponding peak (j) in [6] (21.11 eV) and line (5) in [8], which are not assigned. It should be noted similarities in shape and intensity between peak (j) in [6] and feature (23). In the absence of data from previous literature it is conceivable to attribute its origin to doubly excited states.

The next pair of features (31, 41) at 10.48 and 11.78 eV, respectively, with energy separation 1.30 eV appears in the spectrum as unresolved features. The separation indicates their origins from an excited state which decay to two terms $^2P_{3/2,1/2}$ of the ion core. Energies of the features are: 23.92 eV (10.48 + 13.44) and 23.91 eV (11.78 + 12.13), here and all over the paper the first value in the bracket is the kinetic energy of the ejected electron and the second one the binding energy of the $5p_{1/2,3/2}$ states. These values give a mean energy for the state of 23.915 eV. Delage et al. [6] reported an autoinizing state at 23,91 ± 0.05 eV in Xe energy -loss spectrum, while Codling and Madden [8] presented a transition of 23.895 eV in Xe photoabsorption measurements.

3.1.1 The $5s5p^6 6s(^{3,1}S)$ and $5s5p^6 ns$ (n = 7, 8, 9) autoionizing states

The pairs of features (12, 16) and (13, 19), marked with long dashed lines in Fig. 1a, at energies (6.20, 7.52) and (6.62, 7.92) eV, respectively, with energy separation of 1.32 and 1.30 eV are the pairs that decay to two terms of the ion core. Both pairs are observed from 505 to 40 eV. In a first approach we suppose that the features (12, 13) make a first doublet that decay to the $^2P_{1/2}$ ion core, and the second doublet (16, 19) decays to the $^2P_{3/2}$ ion core. Both doublets have energy separations of 0.42 and 0.40 eV respectively. Energies of the first doublet are: 19.64 eV (6.20 + 13.44) and 20.06 eV (6.62 + 13.44). Energies of the second doublet are: 19.65 eV (7.52 + 12.13) and 20.05 eV (7.92 + 12.13). On that way the lower mean energy of 19.645 eV is attributed to the $5s5p^6 6s(^3S)$ state and energy of 20.055 eV is attributed to the $5s5p^6 6s(^1S)$ state with energy splitting of 0.41 eV. These two pairs of features correspond to the doublets (1, 2), (3, 4) in Xe ejected electron spectrum in experiment of Tweed et al. [5] presented without numerical values of the kinetic energies. Those authors utilized this example in order to show the existence of two series of resonances in ejected spectra of Ar, Kr and Xe, while only one series of resonances is seen in an experiment with scattered electrons used to measure energy positions of the $5s5p^6 6s$ excited states in xenon. Comparison with [5] shows a difference of 0.25 eV for the $6s(^3S)$ and 0.17 eV for the $6s(^1S)$ states, but the splitting is similar (0.41, 0.48) eV. There are no data for the $6s(^3S)$ state from other Ref-s for comparison. However, a good agreement is found between energy of the $6s(^1S)$ (20.055 eV) and data in [4, 6, 38] (20.08, 20.02, 20.08 eV), respectively.

Another possible approach involves the energy comparison of each feature separately with corresponding energies in cited references. The features (12, 13) (6.20, 6.62 eV) have energies close to the energies (6.16, 6.7) eV in [24, Fig. 6] assigned as the resonant Auger lines created by decay of the $4d_{5/2}$ and $4d_{3/2}$ nl photoexcited states, respectively. Also, the features (13, 16, 19) (6.62, 7.52, 7.92) eV have energies in excellent agreement with energies of the peaks labeled as (7b, 9a, 2a) (6.62, 7.53, 7.93) eV taken from Fig. 5 in [22]. The peaks are assigned as the transitions from the Xe $4d_{5/2}6p$ excited states to the $5p^4(^3P_{0,1}, ^3P_2)$ states, respectively (see Table 1). The resonant process occurs at photon energy of 65.11 eV. The electron incident beam may suffer an energy loss equal to the energy needed for the excitation of the $4d_{5/2}6p$ state, however a definite assignment of features (12, 13) to resonat Auger lines would imply a coincidence experiment between the scattered and ejected electrons.

The pair of features (22, 26) (8.41, 9.70) eV appear in the spectrum as a shoulder (22) and a peak (26) with energy separation of 1.29 eV, close to the energy splitting of the ion core, indicating their origin from one single state which decays to two terms of the ion core ($^2P_{3/2,1/2}$). The energies of the corresponding levels are: 21.85 eV (8.41 + 13.44) and 21.83 eV (9.70 + 12.13), what gives a mean energy of 21.84 eV. This energy is attributed to the $7s(^1S)$ state. The comparison shows a good agreement with [4, 6] and the proposed assignment from [4–6] as the $5s5p^6 7s$ state is accepted. It is worth noting that the kinetic energy of the feature (26) is in a very good agreement with the energy of Auger transition N_5-$5s^2 5p^3(^2D)6d(^3S_1)$ from [20, 39]. The same holds for the feature (40) assigned in [20,

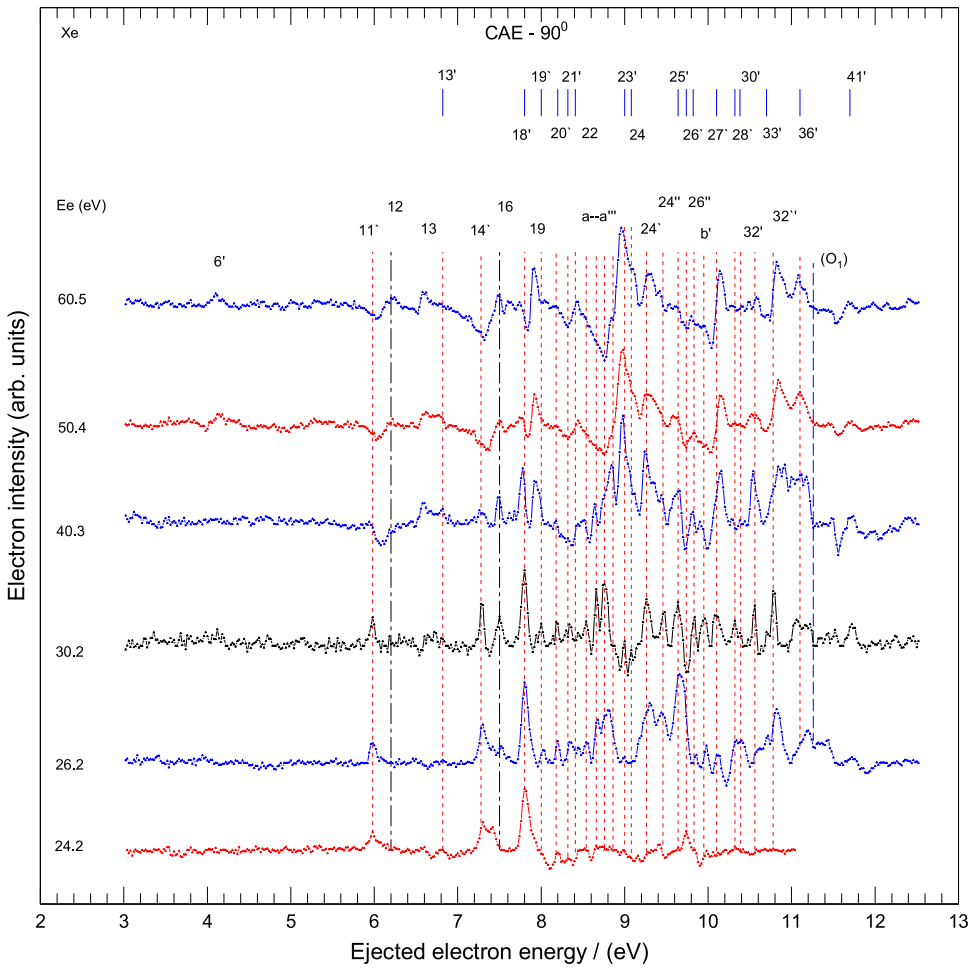

Fig. 2 Series of Xe autoionizing spectra measured at 90° of ejection angle in the kinetic energy region (3–12.5) eV with energy step 0.020 eV. The incident electron energies varies from 60.5 to 24.2 eV. Short full lines on the top of figure and long dashed lines indicate the energy positions of the features

39] as the N_4-$5s^25p^3(^2D)6d(^3S_1)$. So, it is very likely that the intensity of the feature (26) comes from two different processes, one the excitation of the autoionizing state of Xe and the Auger decay of the $4d_{5/2}$ (N_5) orbital.

The features (30, 33) at 10.38 and 10.70 eV, respectively, appear in the spectrum as shoulders with low intensity that makes difficult the identification of their origin. However, if we suppose that the corresponding states decays to the $^2P_{3/2}$ ion core, then their energies (22.51, 22.83) eV are in excellent agreement with calculation [4] where they are assigned as the $5s5p^68s$ and 9 s states, respectively. The excellent agreement in energies is the argument to accept this proposed assignments. In [8] lines (22, 33) also agree excellently in energy, but line (33) was unassigned while line (22) is mentioned as it possibly belongs to the $5p^46s7p$ state.

Another pair of features (28, 37) at 9.96 and 11.26 eV, respectively, with energy separation of 1.30 eV appear in the spectrum with low intensities indicating their origins from an excited state which decays directly to two terms of the $^2P_{3/2,\ 1/2}$ ion core. Energies of the features are: 23.40 eV (9.96 + 13.44) and 23.39 eV (11.26 + 12.13), what gives the mean energy of 23.395 eV. It is worth mentioning that this energy coincides with energy of the O_1 edge of the 5s shell (23.397 eV) assigned as $5s5p^6(^2S_{1/2})$ [11, 15]. But the $5s^{-1}$ ion state cannot decay to the $5p^{-1}$ ground state since they are both ion states and no electron can be emitted. Also, Table 1 shows excellent agreement between this value and unassigned line (60) in [8].

3.1.2 The $5s5p^6np$ (n = 6, 7, 8, 9) autoionizing states

The first optically allowed $5s5p^66p$ state is presented in Fig. 1a as a dip composed from three not resolved shoulders with lower intensities labelled (a–a”’) at energies (8.54, 8.66, 8.76, 8.86) eV, respectively, with energy separation of 100 meV (Table 1). In comparison with the lines in photo absorption measurements [7, 8] one can see a good or excellent agreement in energies. In [7] the $5s5p^66p$ state is presented with four absorption lines from 20.66 to 21.03 eV of binding energies, while in [8] the absorption spectrum shows four lines in this energy region, but the assignments were not given. Only the intense broad line (3) in [8] is identified as the first member of the $5s5p^66p$ state at 20.95 eV. This line should correspond to the minimum of the dip labelled as feature (a”) at 8.76 eV kinetic energy or 20.89 eV binding energy. Energy difference of 60 meV (20.95–20.89) is probably due to the asymmetric shape

of the dip (a"). Two other features (a, a') have an excellent agreement in energies with corresponding lines (1, 2) in [8]. The last feature (a"') at 8.86 eV (20.99 eV) corresponds to the line (4) in [7] at 21.03 eV with energy difference of 40 meV. Based on this, the energy of 20.89 eV is attributed to the $5s5p^6 6p(^1P)$. However, energy position of the $6p(^3P)$ state is not known due to the unknown energy splitting between these states. The energy of the feature (a) (20.67 eV) coincides with the energy of the unassigned peak (h) at 20.67 eV in an energy loss experiment [6, Fig. 3] where the scattered electrons are detected. Also, the energy of the feature (a"') at 8.86 eV is in a very good agreement with calculated energy of 8.88 eV of the line labeled (3) from [26].

The dip (b) at 10.05 eV (22.18 eV) from Fig. 1a is in excellent agreement with the fetures reported in [5, 7] and assigned as the $5s5p^6 7p$ state. Thus we accept this assignment. It should be noted that two values for the energy of the $5p^6 7p$ state, lines (15, 16) (22.19, 22.23) eV with energy separation of 40 meV, are reported in [8] (Fig. 3). The line (15) appearing as a shoulder is in a better agreement with energy of the dip (b) than the line (16). Excellent agreement in energies is found with [20, 39], but their assignment as N_5-$5s^2 5p^3(^2D)6d(^3D_1)$ is not accepted since the dip (b) has been observed until 40 eV incident energy as shown in Fig. 2 in the low incident energy part of this work.

The dip (c) at 10.54 eV (22.67 eV) is assigned to the $5s5p^6 8p$ state due to excellent agreement in energy with [5, 7, 8] and we accept the proposed assignment. Two features lines (27, 28) (22.67, 22.70) eV with energy separation of 30 meV, are also present in Fig. 3 of [8]. The energy of the shoulder (27) is in excellent agreement with dip (c). Good agreement is found with line (5) [20], where the line was left without assignment.

The dip (d) at 10.75 eV, (22.88 eV) is shown in enlarged part of Fig. 1a as a very narrow dip with a width of 60 meV. Its assignment as the $5s5p^6 9p$ state is accepted contrary to discrepancies in energy with corresponding lines from [5, 7, 8] (Table 1) due to its appearance as a dip, a characteristic of all *np* states in the spectrum. Note that Table 1 shows two energies for the 9p state in [8], 23.07 eV taken from Fig. 3 and 22.88 eV taken from Table 2. The second value coincides with energy of the (d). Another coincidence in energy is with the calculated energy 10.75 eV of the feature labeled 6 in [26] and identified as an intense Auger transition. This assignment is not accepted. Excellent agreement is also found with the line (14) in [28], but both lines from [8] and [28] are left without assignments.

The dips (e, f) (11.43, 12.08) eV; (23.56, 24.21) eV have energies above O_1 edge (23.40 eV) and they are left without assignments. The energy of the feature (e), 23.56 eV coincides with the energy of the line (66) in [8] without given assignment and with the energy of the line (s) in [6]. The energy of the feature (f), 24.21 eV, is in excellent agreement with energy of the unassigned line (79) in [8].

3.1.3 The $5s5p^6 nd$ (n = 5–9) autoionizing states

The pair of features (18, 24) (7.78, 9.10) eV have energy separation of 1.32 eV, very close to the energy splitting of the ion core 1.307 eV indicating their origin from one single state which decays to two terms of the ion core ($^2P_{3/2,1/2}$). The energies of the features are: 21.22 eV (7.78 + 13.44) and 21.23 eV (9.10 + 12.13), that gives a mean energy of 21.225 eV. This energy may be attributed to the excited $5d(^3D)$ state, but it is unlikely to detect a triplet state at high incident energy. On the other hand, this assignment is supported by the obtained features at low incident spectra (see Sect. 3.2.3). Tweed et al. [5] assigned line (4) at 21.22 eV in their energy-loss spectrum as the autoionizing $5s5p^6 5d$ states, although they assumed it is the first singlet line in *nd* Rydberg series. Unfortunatelly, they had not observed any higher order line in the series. If the features are treated separately then the energy of the feature (18), 7.78 eV, is in excellent agreement with calculated energy of the Auger transition $4d^{-1}5p^{-1} \rightarrow 5s^{-1}5p^{-2}$ labeled (1) at 7.79 eV in [26]. The energy of the feature (24) at 9.10 eV instead is in good agreement with unassigned line (10) in [28] and close to the calculated energy of the Auger transition $4d^{-2} \rightarrow 4d^{-1}5s^{-1}5p^{-1}$ labeled (4) at 9.21 eV in [26].

The pair of features (20, 25) at 8.00 and 9.32 eV, respectively, with energy separation of 1.32 eV has energies 21.44 eV (8.00 + 13.44) and 21.45 eV (9.32 + 12.13), that gives a mean energy of 21.445 eV. This energy is attributed to the $5s5p^6 5d$ (^1D) excited state. The comparison of this energy with the one in [6, 38] shows an excellent agreement, but discrepancies with the one given in [4, 5]. The energy difference that exists between the $6s(^1S)$ and $5d(^1D)$ is 1.39 eV in this work and may be compared with those in [4] 1.22 eV, [5] 1.34 eV, and [6] 1.36 eV showing very good agreement with [5, 6]. The energy of the $5d(^1D)$ state (21.445 eV) shows good agreement with the unassigned lines in [7, 8]. Also, energy of the feature (20) is in very good agreement with unassigned line (7) in [28].

The features (27, 42) at 9.83 and 11.87 eV, respectively, form a pair with an energy separation 2.04 eV. The feature (27) is still visible at 26 eV, while the (42) one vanishes at 60 eV (Fig. 2). So, if we treat the peak (27) independently as an autoionizing level of energy 9.83 + 12.13 eV that would give an energy of the state 21.96 eV, that does not correspond to the value of 22.30 eV as calculated energy for the 5s → 6d transition in [4]. On the other hand a comparison with other energies shows that both features have kinetic energies in good agreement with corresponding unassigned lines (12, 17) in [28].

Feature (32) at 10.59 eV is present in the spectrum with high intensity and it vanishes below 26 eV. If the corresponding autoionizing state decays to the $^2P_{3/2}$ ionic state, then its energy is 22.72 eV, in a very good agreement with [4, 6] and the assignment $5s5p^6 7d$ from [4, 6] is accepted for this feature. We should note an

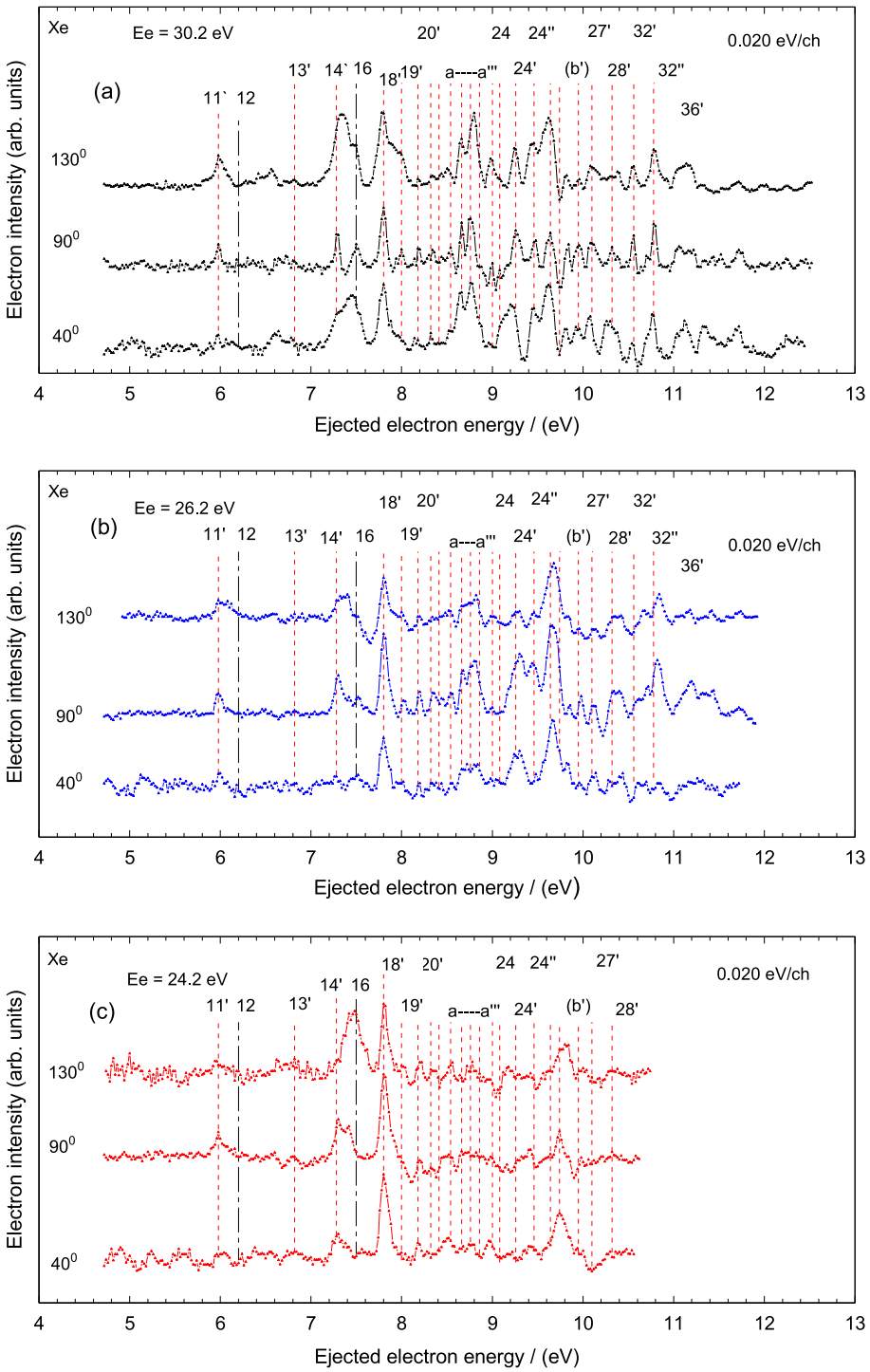

Fig. 3 Series of the three Xe autoionizing spectra in the kinetic energy region 4.5 to 12.5 eV measured in the CAE mode at incident energies 30.2 eV (**a**), 26.2 (**b**) and 24.2 (**c**) and at three ejection angles (40°, 90°, 130°). The energies of the features are listed in Table 2

excellent agreement with the line (5) in [20], assigned as the N_5—$5s^25p^3(^2D)6d\ ^3D_1$ transition.

The next pair of features (34, 43) at 10.83 and 12.15 eV, respectively, with energy separation of 1.32 eV appear in the spectrum with different intensities. Feature (34) is a very intense broad feature, while feature (43) is visible only in the expanded view of the spectrum. The energy separation indicates the origin from an excited state which decay to two terms $^2P_{3/2,1/2}$ of the ion core. The energy of the state is 24.275 eV (mean value) (10.83 + 13.44) and (12.15 + 12.13). This energy is in a good agreement with the energies assigned to the Auger transition N_4-$5s^15p^5\ ^3P_2$ in [20, 39] and the unassigned line (80) in [8]. On the other hand, if we assume that the feature (34) is coming from the decay to the ground level of Xe^+, its autoionizing energy would be 22.96 eV which can be assigned as the $5s5p^68d$ [4, 6].

Table 2 Kinetic energies (KE) (eV), Binding energies (eV)* of the peaks from the Xe ejected electron spectra of at low incident energy taken from Fig. 2

Peak N^0 KE(eV)	Energy separation between peaks ΔE (eV)	[Ref.], Line, Assignment	Kin. En. (eV) or (Binding. En.) (eV)*
6′ 4.10			
11′ 5.98 14′ 7.28	(11'–14'): 1.30 (11'–12): 0.22	[This work], (11', 12): $5s5p^6 6s(^3S)$	19.415* (PCI)
12 6.20 16 7.50	(12–16): 1.30 (14'–16): 0.22	[This work], (14', 16): $5s5p^6 6s(^1S)$	19.635*
13′ 6.82 20′ 8.18	(13'–20'): 1.36	[This work], (13', 20'): . . . /. [6], (g) . . . /.	20.285* 20.28*
18′ 7.80 24 9.08	(18'–24): 1.28	[This work], (18', 19'): $5s5p^6 5d(^3D)$	21.225*
19′ 8.00 24′ 9.26	(19'–24'): 1.26	[This work], (24, 24'): $5s5p^6 5d(^1D)$	21.415*
21′ 8.32 25′ 9.64	(21'–25'): 1.32	[This work], (21', 22): $5s5p^6 7s(^3S)$	21.765*
22 8.41 26′ 9.74	(22–26'): 1.33	[This work], (25', 26'): $5s5p^6 7s(^1S)$	21.86*
a 8.54 a" 8.76		[This work], (a, a"): $5s5p^6 6p(^{3,1}P)$	(20.67, 20.89)*
a' 8.66 b' 9.95	(a'–b'): 1.29	[This work], (a', b'): . . . /. [6], (m) . . . /.	22.09* 22.10*
23′ 9.00 28′ 10.32	(23'–28'): 1.32	[This work], (23', 28'): . . . /. [6], (o) . . . /.	22.445* 22.45*
30′ 10.39		[This work], 30': $5s5p^6 8s(^1S)$ [4], $5s5p^6 8s$	22.52* 22.52*
27′ 10.10		[This work], 27': $5s5p^6 6d$ [4, 6], (. . . /., n): $5s5p^6 6d$	22.23* (22.30, 22.30)*
32′ 10.56		[This work],: $5s5p^6 7d$	22.69*
33′ 10.70		[This work], 33': $5s5p^6 9s$	22.83*
24" 9.46 32" 10.78	(24"–32"): 1.32	[This work], (24", 32"): $5s5p^6 8d$ [4],: $5s5p^6 8d$	22.905* 22.95*
26" 9.82 36′ 11.10	(26"–36'): 1.28	[This work], (26", 36'): $5s5p^6 12d$ [4],: $5s5p^6 12d$ [6], (r) . . . /.	23.245* 23.24* 23.26*
41′ 11.70		[6], (t) . . . /.	23.91*

Binding energy (BE)* = (KE + 12.13) eV
(*) Binding energy, (Excit. Energy)

Feature (35) at 10.93 eV is present in the spectrum as a shoulder on the higher energy side of feature (34) making this common feature broad and intense. It vanishes below 40 eV (Fig. 3). Supposing that corresponding state decays to the $^2P_{3/2}$ ion core (12.13 eV), its energy is 23.06 eV. Feature (35) has an excellent agreement with the calculation in [4, 7, 8] and a very good agreement with [20]. The assignment from [4] may be accepted and energy of 23.06 eV is attributed to the $5s5p^6 9d$ state.

Feature (36) at 11.08 eV is present in spectra with low intensity and at all incident energies down to 30 eV (Fig. 2). If the corresponding state decays to the $^2P_{3/2}$ ion core (12.13 eV), its energy at 23.21 eV coincides with the calculations in [4] which assign it as the $5s5p^6 11d$ state. This assignment is accepted. The excellent agreement is also found with line (48) in [8] and with the unassigned lines in [6, 28].

3.1.4 Features of higher kinetic energies

The features (38, 39) at 11.52 and 11.61 eV, respectively, appear in the spectrum with low intensity. Electron with such energies can be released from the autoionizing states which energies are 23.65 and 23.74 eV, respectively. The autoionizing states with

these energies had not been observed in [8]. An unassigned feature at 23.7 eV was found in Xe 5s photoelectron high resolution spectrum in [15]. The feature (8) at 11.55 eV was identified in [20] as the N_5-$O_1O_{2,3}$ Auger transition that corresponds to the optical feature at 11.57 eV assigned as the N_5-$5s^25p^3(^2P)6p\ ^3D_3$.

Feature (40) at 11.72 eV is visible in the spectrum as a part of the broad peak not resolved from two other features. It appears from 60 down to 26 eV incident energy (Fig. 2), indicating its origin probably from doubly excited states. The kinetic energy is in a very good agreement with corresponding line (9) in [21, 39] labeled as N_4-$5s^25p^3(^2D)6d\ ^3S$ transition, but the assignment is not accepted, because the feature is observed below the 4d ionization energy.

The next two features (44, 45) at 12.26 and 12.45 eV, respectively, are shown in the spectrum with low intensities. The kinetic energy of feature (44) coincides with the calculated energy 12.26 eV of the Auger transition labeled (7) in [26], thus the proposed assignment is accepted. The binding energy of feature (45) (24.58 eV) is in excellent agreement with the unassigned line 88 in [8].

The next four features (46, 47, 48, 49) at 12.60, 12.68, 12.76, and 12.84 eV, respectively, are shown in the spectrum as not resolved broad peak with feature (47) corresponding in some cases to a maximum and in others to shoulders. Similarly to previous cases, if the corresponding states decay to the $^2P_{3/2}$ ion core, then energies of the states are (24.73, 24.81, 24.89, 24.97) eV, respectively. Energies of the features (46, 47, 49) coincide with unassigned lines (93, 95, 99) in [8]. Feature (46) has an excellent agreement of the binding energy 24.73 eV of unassigned line (93) [8]. The kinetic energy of feature (47) also coincides with the energy of the unassigned line (19) in [28]. The kinetic energy of feature (48) corresponds to line (28) at 12.54 eV in Werme et al. [36] which energy was corrected to 12.741 eV by Carroll et al. [37]. Persson et al. [39] calculated the energy of the $5s^25p^3(^2P)5d\ ^1P_1$ state of Xe^{2+} to be 21.704 eV what is the final state of the process where the hole in $d_{5/2}$ orbital produces an Auger electron with 12.739 eV kinetic energy. This assignment of the final state was adopted in [19, 20, 31] for the Auger electrons of energy 12.72, 12.58 and 12.77 eV, respectively. The kinetic energy of feature (49) is in excellent agreement with energy of the line (3) in [20] and line (20) in [28]. The line (3) in [20] was assigned to the N_5 -$5p^35d$ transition, that is accepted for this feature, while the line (20) in [28] was left without assignment.

The feature (50) at 12.96 eV is a visible peak in enlarged spectrum in Fig. 1a. It has a good agreement in energy with the first step Auger cascade transition $4d_{5/2}6p \rightarrow 5s^05p^6(^1S)6p$ line at 12.99 eV in [23].

The features (51, 52, 53) at 13.06, 13.12 and 13.18 eV, respectively, are not completely resolved in Fig. 1a due to the limited experimental resolution. If the corresponding states decay to the $^2P_{3/2}$ ion core (12.13 eV), their energies are 25.19, 25.25, 25.31 eV, respectively. The features (51, 52) have excellent agreement of energy with unassigned autoionizing lines (108, 109) in [8]. The energy of feature (53) is in excellent agreement with [8] and the kinetic energy is in very good agreement with [20, 24, 28].

The features (54, 55, 56) at 13.32, 13.54 and 13.64 eV, respectively, are shown in the spectrum as isolated peaks with low intensity. Electron with such energies can be released from the autoionizing states which energies are 25.45, 25.67 and 25.77 eV, respectively. The energy of peak (54) is in good agreement with one in [8]. The energy of feature (55) is in good agreement with unassigned autoinizing line (124) in [8]. The energy of the autoionizing state that gives feature (56) (25.77 eV) is in a very good agreement with unassigned line (126) in [8].

3.2 Autoionizing states of xenon at low incident electron energies

In the present work we studied autoionizing states of xenon at low incident electron energies from 60 down to 24 eV i.e., energy region between ionization of the 5s state (23.40 eV) and Xe^{3+} (64.09 eV) in limited kinetic energy region (3–12.5) eV. This energy region covers only single and doubly excited states, but not contributions from the Auger electrons produced in the ionization of the 4d inner shell (67–69 eV binding energy). The main aim is to identify triplet states and to obtain their energies.

Figure 2 shows series of the autoionizing spectra of xenon obtained in the CAE mode at 90° in kinetic energy region (3–12.5) eV and various electron incident energies from 24.2 to 60.5 eV. The first feature (6') at 4.10 eV coincides with energy of line at 4.1 eV in [24] defined as $4d_{3/2}$ Auger line, but the figure shows that the feature vanishes at around 40 eV incident energy, an energy lower than the binding energy of the 4d state. This exclude the assignment as a slow Auger electron produced in a cascade process.

3.2.1 The $5s5p^66s(^{3,1}S)$ and $5s5p^6(7s, 8s, 9s)$ states at low incident electron energies

Energies of the first excited $5s5p^66s(^{3,1}S)$ states at 19.645 and 20.055 eV, respectively, have been already observed at a high incident energy (Fig. 1a). These states appear in the spectra as two doublets that decay to two terms $^2P_{3/2,\ 1/2}$ of the ion core. In the low incident energy region between 40 and 60 eV these two doublets are still observed as peaks, while at energies between 40 and 24 eV they are transformed in two other well defined peaks (11', 14') at 5.98 and 7.28 eV, respectively, with energy separation of 1.30 eV. Another pair of features (12, 16) at 6.20 and 7.50 eV, respectively, have also an energy separation of 1.30 eV. These two pairs can form two doublets (11', 12) and (14', 16) with energy separation of 0.22 eV, shown in Fig. 2 with long dashed lines. The energies of the doublets are 19.42 eV (5.98 + 13.44) and 19.64 eV (6.20 + 13.44) for the first doublet and 19.41 eV (7.28 + 12.13) and 19.63 eV (7.50

+ 12.13) for the second doublet. Hence, the energies of 19.415 eV and 19.635 eV (mean values) correspond to the $5s5p^6 6s(^{3,1}S)$ states. A comparison between the results of the experiments at high and low incident energies shows discrepancies of 0.230 and 0.420 eV, respectively. There is also a discrepancy between the value of the spin orbit splitting 0.22 eV at low incident energy and 0.4 eV at high incident energy. It is unlikely that an explanation for this shift may be due to the PCI effect between the ejected and incident/scattered elctrons. Finally, we accept energies of the triplet and singlet states obtained at high incident energies (19.645, 20.055) eV and spin orbit splitting of 0.4 eV. Comparison with other references is shown in Table 1. Note that energy of the triplet state 19.415 eV is in good agreement with energy of the triplet state 19.40 eV in [5].

Angular dependences of the features (11', 14') at incident energies at 30.2, 26.2 and 24.2 are shown in Fig. 3a, b and c in kinetic energy region (4.8–12.4) eV. Figures show that feature (11') has no angular dependence at all three energies, while feature (14') shows angular dependence. The feature changes shape with ejection angle that indicates an interference effect between the ejected electron from the autoionizing process and the scattered one in the ionization process.

The pair of features (21', 25') at 8.32 and 9.64 eV, respectively, with energy separation of 1.32 eV are shown in the spectrum as two peaks at incident energies 30.2 and 26.2 eV (Fig. 2). Another pair of features (22, 26') at 8.41 and 9.74 eV, respectively, with energy separation of 1.33 eV are present in the spectra (Fig. 2), the first one is observed with low intensity, while the second one appears as a minimum until the incident energy of 30.2 eV and then as a peak at energies of 26.2 and 24.2 eV. As in the case of the 6s state, these two pairs (21', 25'), (22, 26') are created from a state which decays to two terms of the $^2P_{3/2,1/2}$ ion core in form of the two doublets, the first (21', 22) and a second (25', 26'). Energies of the first doublet are: (21.76, 21.85) eV and of the second doublet (21.77, 21.87) eV. So, the lower mean energy 21.765 eV corresponds to the $5s5p^6 7s(^3S)$ state and mean value of 21.86 eV to the $5s5p^6 7s(^1S)$ state with unknown core spin—orbit splitting. A comparison with high incident energies shows an excellent agreement for the energy of the singlet state, while the triplet state is absent at high energies. This shows the importance of measurements at low incident energies in order to get a definite evidence of the $7s(^3S)$ state.

The angular dependence of these four features is shown in Fig. 3. Feature (21') is present at all three energies with low intensity, while feature (25') is present as a broad not resolved peak. Feature (22) is present with low intensity at all energies and angles, while feature (26') is a dip at 30.2 eV at all three angles and becomes a broad peak at 26.2 and 24.2 eV at all three angles.

Feature (30') at 10.39 eV appears in the spectrum (Fig. 2) with low intensity. Supposing that the corresponding state decays to the $^2P_{3/2}$ ion core (12.13 eV), its energy is 22.52 eV (10.39 + 12.13) attributed to the $5s5p^6 8s(^1S)$ state. The comparison is only possible with calculation in [4] and an excellent agreement (22.52 eV) is found. Comparison with the high incident energy data of this work shows excellent agreement. The comparison of the energy difference between the 7s and 8s states in this work (0.67 eV) and in [4] (0.72 eV) shows fair agreement.

Feature (33') at 10.70 eV appears in the spectrum with low intensity at incident energies 30 and 26 eV. If the corresponding state decays to the $^2P_{3/2}$ of the ion core, then its energy is 22.83 eV. This energy is in excellent agreement with calculation in [4] (22.85 eV) assigned to the $5s5p^6 9s$ state. This energy is in good agreement with the unassigned line (33) in [8]. The comparison with high energy data shows excellent agreement as far as the energies are concerned. Energy difference of 0.31 eV between the 8 s and 9 s states in this work is in excellent agreement with calculation in [4] (0.33 eV).

The two features (13', 20') at 6.82 and 8.18 eV, respectively, with energy separation of 1.36 eV are shown in the spectrum at incident energies below 40 eV with low intensity, but well separated. Their energies are 20.26 and 20.31 eV (6.82 + 13.44) and (8.18 + 12.13), respectively, with the mean energy of 20.285 eV. This value is in excellent agreement with the energy of the unassigned peak (g) in [6] (20.28 eV) obtained at 50 eV of incident energy. In the present work the two features appear at low incident energies only, and we suggest that their origin is from a doubly excited state which decays to two terms of the ion core. Angular dependence of these two features is shown in Fig. 3. The feature (13') is present with low intensity at all energies and angles. However it is difficult to follow its angular dependence. Feature (20') is present at all three energies and ejection angles with the same shape showing no angular dependence.

3.2.2 The $5s5p^6$(6p, 7p, 8p) excited states at low incident energies

The $5s5p^6 6p$ state shows up as a dip with shoulders at high incident energy of 505 eV as well as at low energies 60.5 and 50.4 eV (Fig. 2). At lower incident energies the dip is replaced by four peaks at 40.3 eV and three peaks with shoulder at 30.2 and 26.2 eV. The peaks have the same kinetic energies as dips observed at 505 eV incident energy. This was the reason to keep the same labels (a–a'') in Table 2. In the 30.2 eV spectrum the first (a) and the last peak (a'') display low intensities, while the two (a', a'') in the middle appear with higher intensities and almost separated. Their intensities are unusual for optically allowed transitions at low incident energy indicating the contribution from another state overlapping in energy, probably a doubly excited state. That state is represented by two peaks at kinetic energies

8.66 eV (a') and 9.95 eV (b') (Fig. 2) with an energy separation of 1.29 eV, which indicates a decay to both terms $^2P_{3/2,\,1/2}$ of the ion core. The energies of the peaks are: 22.10 eV and 22.08 eV or 22.09 eV as a mean value. A state with this energy is not identified among the singly excited states. This suggests its origin from doubly excited states. Comparison with the peak (m) at 22.10 eV in [6] shows excellent agreement, but no assignment has been given. This shows that energy of the 6p state cannot be defined precisely at low incident energy. The angular dependence of the peaks (a', b') is shown in Fig. 3. Both peaks do not show angular dependence at 30.2 and 26.2 eV, but their intensities and resolution decrease at 26.2 eV. The peak (a") has no angular dependence and the experimental resolution does not allow to obtain more details. Unfortunately, there are no data of the states with similar or equal energies from other electron spectra in literature for comparison.

The $5s5p^6 7p$ state already identified at high incident energy as a dip (b) at 10.05 eV is also present in Fig. 2 at the same kinetic energy in spectra from 60 to 40 eV of incident energies and it vanishes below 30 eV. So, this state is shown in the spectrum until 40 eV at the same energy as at 505 eV (22.18 eV).

The $5s5p^6 8p$ state identified at high incident energy as a dip (c) at 10.54 eV (22.67 eV) is replaced by a peak at 60–26 eV incident energies (Fig. 2). The higher intensity of the peak at 40.3 and 30.2 eV comes from another state identified as the 7d state at energy 10.56 eV (22.69 eV) shown with long dashed line (32') in Fig. 3. So, the observation of the 8p state cannot be confirmed at low incident energies.

3.2.3 The $5s5p^6$(5d, 6d, 7d, 8d) states

Identification of both $5d(^{3,1}D)$ states is easier at low incident energies than at high incident energies because the intensity of the triplet state is dominant. The 5d state appears as two doublets which decay to the two terms $(^2P_{3/2,\,1/2})$ of the ion core. The first doublet is (18', 19') at 7.80 and 8.00 eV, respectively, and the second doublet (24, 24') at 9.08 and 9.26 eV, respectively, with energy separations (1.28, 1.26) eV, respectively (Fig. 2). The energies of the first doublet are 21.24 and 21.44 eV and of the second doublet 21.21 and 21.39 eV. The lower energies 21.24 and 21.21 eV with mean value of 21.225 eV corresponds to the $5s5p^6 5d(^3D)$ state and the higher ones (21.44 and 21.39) eV with mean value of 21.415 eV corresponds to the $5s5p^6 5d(^1D)$ state with a spin orbit splitting of 0.190 eV. No comparison of energy for the $5d(^3D)$ state is done with other Ref-s due to the absence of data. The comparison of energy for the $5d(^1D)$ state shows discrepancies with calculation in [4, 5], but good agreement with [6, 38] (Table 1). The comparison with our spectrum at high incident energy shows excellent agreement for the $5s5p^6 5d(^3D)$ state and difference of 30 meV for the $5s5p^6 5d(^1D)$ state. Angular dependence of these four features is shown in Fig. 3. The features (18', 19') do not show angular dependence except for the intensity of the feature (19'). The behavior of the two other features (24, 24') is complex, feature (24) has very low intensity and its angular dependence can be extracted, while feature (24') shows an intensity variation.

Feature (27') at 10.10 eV is present in the spectra as a peak only at the lowest incident energies 30.2 and 20.2 eV (Fig. 2), while at higher incident energies 40.3–60.5 eV it is a part of a broad feature. This peak is a part of feature (29) at 505 eV with a maximum at 10.22 eV. Thus feature (27') is attributed to the $5s5p^6 6d$ state at energy 22.23 eV (10.10 + 12.13) supposing that the state decays to the $(^2P_{3/2})$ of the ion core. At high incident energy (505 eV), the 6d state is not identified due to insufficient experimental resolution and is part of the broad feature (29) (10.22 eV). A good agreement in energy (see Table 2) is found with both the calculation in [4] and the peak (n) in [6]. As for the angular dependence is concerned the peak is observed at all angles in Fig. 3a, b, but is absent in Fig. 3c. The energy difference between the 6d and 5d states in this work is 0.815 eV, different from the 1.0 eV of [4] and 0.92 eV of [6].

Feature (32') at 10.56 eV is shown as a peak in Fig. 2 at the incident energies from 50.4 to 30.2 eV. Supposing that the state decays to the $(^2P_{3/2})$ of the ion core then the energy of the (32') is 22.69 eV (10.56 + 12.13) and is identified as the $5s5p^6$ 7d state. As it was mentioned in the case of the $5s5p^6 8p$ state (10.54 eV) the experimental resolution is not enough to separate the 8p and 7d states, thus making uncertain their contribution to the intensity of the peak. However a higher contribution from the 7d state should be expected. Comparison with the high incident energy data (Table 1) shows an energy difference of 30 meV, comparable to the uncertainty of 20 meV of our data. Comparison of the measured energy with calculations in [4] and [8] (Table 1) shows an excellent agreement. Figure 3a shows no angular dependence of this peak at 30.2 eV of incident energy. The energy difference of 0.46 eV between 6d and 7d in this work is in good agreement with calculated 0.4 eV in [4] and 0.43 eV in [6].

The next pair of features (24", 32") at 9.46 and 10.78 eV, respectively, with an energy separation of 1.32 eV belongs to a state which decays to two terms $(^2P_{3/2,\,1/2})$ of the ion core. They are present as peaks at 30.2 eV spectrum. Energies of the features are: 22.90 eV (9.46 + 13.44) and 22.91 eV (10.78 + 12.13), that gives a mean energy of (22.905 ± 0.020) eV identified as the $5s5p^6$ 8d state. Only the comparison with calculation in [4] shows a fair agreement with an energy difference of 45 meV (Table 2). Comparison between energy of the (32") with energy of the dip (d) 10.75 eV in the high incident energy data identified as the $5s5p^6 9p$ shows an energy difference of 30 meV. Therefore it is not possible to resolve the 8d and 9p states, which according references [3] and [4] should be separated by 10 meV. So, the low experimental resolution prevents the identification of the 8d state at high incident energy. The energy difference of 0.21 eV between the 7d and 8d

states measured in this work is in very good agreement with the calculated value of 0.25 eV in [4]. The features (24", 32") are present at all angles at 30.2 and 26.2 eV spectra (Fig. 3).

The pair of features (23', 28') at 9.00 and 10.32 eV, respectively, with energy separation of 1.32 eV comes from one state which decays to two terms ($^2P_{3/2,\ 1/2}$) of the ion core. Energies of the features are (22.44, 22.45) eV (9.00 + 13.44) and (10.32 + 12.13) eV. The mean energy of 22.445 eV is attributed to the doubly excited state, but the state is not found in Ref-s and the feature is left without assignment. The comparison with unassigned peak (o) at 22.45 eV in [6] shows an excellent agreement in energy.

The last pair of features (26", 36') at 9.82 and 11.10 eV, respectively, have energy separation of 1.28 eV. They represent a state which decays to the two terms of the ion core. The energy of the state can be calculated as in previous cases using this separation. The energies of the features are 23.26 eV (9.82 + 13.44) and 23.23 eV (11.10 + 12.13), that gives the mean value of 23.245 eV. This energy is in excellent agreement with the calculated value of 23.24 eV in [4] assigned as the $5s5p^6 12d$ state and with the unassigned peak (r) at 23.26 eV in [5]. We are not sure about the assignment from [4] because the high intensity of the feature (36') cannot be only due the 12d state and certainly it comes from contribution of another not resolved closely spaced feature below O_1 edge (23.40 eV). Comparison with feature (36) at 23.21 eV in high incident energy spectrum shows energy difference of 35 meV.

The ionization energy of the 5s state (O_1) edge (23.40 eV) is indicated with dashed line in Fig. 2 and appears as cusp in the spectrum, especially at energies 50.4, 40.3, 30.2 eV and it can be used as a calibration energy. This agreement supports accuracy of our calibration of the kinetic energy.

Feature (41') at 11.70 eV appears as a peak at energies 60.5–26.2 eV in Fig. 2. Energy of this feature (23.83 eV) supposing that the corresponding state decay to the $^2P_{3/2}$ ion core (12.13 eV) is above O_1 edge (23.40 eV) indicating its origin from doubly excited state.

4 Conclusions

The Xe autoionizing spectra obtained at high (505, 2019 eV) and low incident energies (60–24) eV were studied systematically by using a high-resolution electrostatic analyzer and non- mononochromatic electron beam. In a high energy region, a large number of features that comes from singly, doubly excitation, correlation satellites and slow Auger electrons is analyzed and assigned. It is found that the $5s5p^6(6s, 5d)$ states appear in the spectra as two doublets which decay to two terms of the ($^2P_{3/2,\ 1/2}$) ion core. Energies of the states $6s(^{3,1}S)$ (19.645, 20.055) eV, $5d(^{3,1}D)$ (21.225, 21.445) eV and spin orbit splitting (0.410, 0.220) eV, respectively, are determined and compared with other data from literature. In spectra at low incident electron energies, the existence of the $6s(^{3,1}S)$ states at 19.415 and 19.63 eV, respectively, with spin orbit splitting of 0.215 eV is confirmed, but here the energies of the ejected electrons are influenced by the PCI effect. Also, the states $7s(^{3,1}S)$ (21.765, 21.85) eV and $5d(^{3,1}D)$ (21.225, 21.415) eV and corresponding spin orbit splitting of 0.085 and 0.190 eV, respectively, are found. Angular dependences for some of the states are presented at 40°, 90° and 130°. The comparison of obtained data with data from literature shows good or excellent agreement.

Acknowledgements The work has been performed under the project OI 171020 of MESTD of Republic of Serbia and within the scope of bilateral project between Italy and Serbia of particular relevance (Grande Rilevanza) "Nanoscale insights in radiation damage". J. J. J, is grateful to the Institute of Physics Belgrade for using their material resourses.

Author contribution

All authors contributed to the study conception and design. Material preparation and data collection was done by Jozo Jureta, while the analysis was performed by all authors. The first draft of the manuscript was written by Jozo Jureta and all authors contributed to the final manuscript. All authors read and approved the final manuscript.

Data availability This manuscript has no associated data or the data will not be deposited. [Authors' comment: All data generated or analysed during this study are included in this published article.]

Declarations

Conflict of interest The author declare that they have no conflict of interest.

References

1. T.D. Märk, G.H. Dunn (eds.), *Electron impact ionization*, 1st edn. (Springer, Vienna, 1985)
2. L. Avaldi, P. Belotti, P. Bolognesi, R. Camilloni, G. Stefani, Phys. Rev. Lett. **75**, 1915 (1995)
3. J.J. Jureta, B.P. Marinković, L. Avaldi, Adv. Space Res. **71**, 1338 (2023)
4. C.E. Brion, L.A.R. Olsen, J. Phys. B **3**, 1020 (1970)
5. R.J. Tweed, F. Gelebart, J.J. Peresse, J. Phys. B **9**, 2643 (1976)
6. A. Delage, D. Roy, J.D. Carette, J. Phys. B **10**, 1487 (1977)
7. J.A.R. Samson, Phys. Lett. **8**, 107 (1964)
8. K. Codling, R.P. Madden, J. Res. Nat. Bur. Stand A **76**, 1–12 (1972)
9. U. Gelius, J. Electron Spectrosc. Relat. Phenom. **5**, 985 (1974)

10. S. Svensson, B. Eriksson, N. Mårtensson, G. Vendin, U. Gelius, J. Electron Spectrosc. Relat. Phenom. **47**, 327 (1988)
11. M. Carlsson-Gothe, P. Baltzer, P. Wannberg, J. Phys. B **24**, 2477 (1991)
12. E. Hansen, W. Persson, Phys. Scr. **36**, 602 (1987)
13. A. Fahlman, M.O. Krause, T.A. Carlson, A. Svensson, Phys. Rev. A **30**, 812 (1984)
14. M.O. Krause, S.B. Whitfield, C.D. Caldwell, J.Z. Wu, P. van der Meulen, C.A. de Lange, R.W.C. Hansen, J. Electron Spectrosc. Relat. Phenom. **58**, 79 (1992)
15. C.E. Brion, A.O. Bawagan, K.H. Tan, Can. J. Chem. **66**, 1877 (1988)
16. S. Southworth, U. Becker, C.M. Truesdale, P.H. Kobrin, D.W. Lindle, S. Qwaki, D.A. Shirley, Phys Rev. A **28**, 261 (1983)
17. A.A. Wills, A.A. Cafolla, J. Comer, J. Phys. B **23**, 2029 (1990)
18. A. Kikas, S.J. Osborne, A. Ausmees, S. Svensson, O.P. Sairanen, S. Aksela, J. Electron Spectrosc. Relat. Phenom. **77**, 241 (1996)
19. A. Kivimäki, L. Pfeiffer, H. Aksela, E. Nommiste, S. Aksela, J. Electron Spectrosc. Relat. Phenom. **101–103**, 43 (1999)
20. J. Jauhiainen, H. Aksela, S. Aksela, A. Kivimäki, O.P. Sairanen, E. Nommiste, J. Vegh, J. Phys. B **28**, 3831 (1995)
21. S. Alitalo, A. Kivimäki, T. Matila, K. Vaarala, H. Aksela, S. Aksela, J. Electron Spectrosc. Relat. Phenom. **114–116**, 141 (2001)
22. S. Huttula, S. Heinäsmäki, H. Aksela, E. Kukk, M. Huttula, S. Aksela, Phys. Rev. A **67**, 052703 (2003)
23. K. Ueda, Y. Shimizu, H. Chiba, M. Kitajima, M. Okamoto, M. Hoshino, H. Tanaka, T. Hayaishi, S. Fritzsche, I.P. Sazhina, N.M. Kabachnik, J. Phys. B **36**, 319 (2003)
24. P. Lablanquie, S. Sheinerman, F. Penent, R.I. Hall, M. Ahmad, T. Aoto, Y. Hikosaka, K. Ito, J. Phys. B **35**, 3265 (2002)
25. F. Penent, J. Palaudoux, P. Lablanquie, L. Andric, R. Feifel, J.H.D. Eland, Phys. Rev. Lett. **95**, 083002 (2005)
26. V. Jonauskas, L. Partanen, S. Kučas, R. Karazija, M. Huttula, S. Aksela, H. Aksela, J. Phys. B **36**, 4403 (2003)
27. U. Becker, D. Szostak, H.G. Kerkhoff, B. Langer, R. Wehlitz, A. Yagishita, T. Hayaishi, Phys. Rev. A **39**, 3902 (1989)
28. H. Aksela, S. Aksela, H. Pulkkinen, Phys. Rev. A **30**, 865 (1984)
29. G.C. King, M. Tronc, F.H. Read, R.C. Bradford, J. Phys. B **10**, 2479 (1977)
30. K.G. Dyall, F.P. Larkins, J. Phys. B **15**, 219 (1982)
31. I.D. Petrov, B.M. Lagutin, V.L. Sukhorukov, A. Ehresmann, H. Schmoranzer, J. Phys. B **47**, 055001 (2014)
32. S. Braidwood, M. Brunger, E. Weigold, Phys. Rev. A **47**, 2927 (1993)
33. M.J. Brunger, S.W. Braidwood, I.E. McCarthy, E. Weigold, J. Phys. B **27**, L597 (1994)
34. J.J. Jureta, A.R. Milosavljević, B.P. Marinković, Int. J. Mass Spectrom. **365–366**, 114 (2014)
35. J.J. Jureta, B.P. Marinković, L. Avaldi, Eur. Phys. J. D. **70**, 199 (2016)
36. L.O. Werme, T. Bergmark, K. Siegbahn, Phys. Scr. **6**, 141 (1972)
37. T.X. Carroll, J.D. Bozek, E. Kukk, V. Myrseth, L.J. Saethre, T.D. Thomas, K. Wiesner, J. Electron Spectrosc. Relat. Phenom. **125**, 127 (2002)
38. T. Bergmark, K. Spohr, N. Magnusson, L.O. Werme, C. Nordling, K. Siegbahn. Inst. Phys. Uppsala Univ. Report N° 589, (1969)
39. W. Persson, C.-G. Wahlstram, G. Bertuccelli, H.O. Di Rocco, I.G. Reyna Almandos, M. Gallardo, Phys. Scr. **38**, 347 (1988)